
Clinical Implementation of Adaptive Helical Tomotherapy: A Unique Approach to Image-Guided Intensity Modulated Radiotherapy

www.tcrt.org

Image-guided IMRT is a revolutionary concept whose clinical implementation is rapidly evolving. Methods of executing beam intensity modulation have included individually designed compensators, static multi-leaf collimators (MLC), dynamic MLC, and sequential (serial) tomotherapy. We have developed helical tomotherapy as an innovative solution to overcome some of the limitations of other IMRT systems. The unique physical design of helical tomotherapy allows the realization of the concepts of adaptive radiotherapy and conformal avoidance. In principle, these advances should improve normal tissue sparing and permit dose reconstruction and verification, thereby allowing significant biologically effective dose escalation.

Recent radiobiological findings can be translated into altered fractionation schemes that aim to improve the local control and long-term survival. This strategy is being tested at the University of Wisconsin using helical tomotherapy with its highly precise delivery and verification system along with meticulous and practical forms of immobilization. Innovative techniques such optical guidance, respiratory gating, and ultrasound assessments are being designed and tailored for helical tomotherapy use. The intrinsic capability of helical tomotherapy for megavoltage CT (MVCT) imaging for IMRT image-guidance is being optimized.

The unique features of helical tomotherapy might allow implementation of image-guided IMRT that was previously impossible or impractical. Here we review the technological, physical, and radiobiological rationale for the ongoing and upcoming clinical trials that will use image-guided IMRT in the form of helical tomotherapy; and we describe our plans for testing our hypotheses in a rigorous prospective fashion.

Key words: Tomotherapy; IMRT; Adaptive radiotherapy; Conformal avoidance; Hypofractionation; and Accelerated fractionation.

Introduction

There has been a recent transition in radiation oncology from standard treatment planning and targeting approaches to more advanced approaches based on significant improvements in imaging and treatment delivery, resulting in innovative approaches to image-guided radiotherapy such as helical tomotherapy (1). Here, we review some of the innovations in clinical application that have become feasible as a consequence of these new technologies. We specifically focus on the potential of helical tomotherapy-based intensity modulated radiotherapy (IMRT), which we have developed.

IMRT represents a major paradigm shift in radiation oncology and its clinical application is still evolving. As more institutions implement IMRT, deci-

James S. Welsh, M.S., M.D.,^{1,5,*}
Michael Lock, M.D.²
Paul M. Harari, M.D.¹
Wolfgang A. Tomé, Ph.D.^{1,6}
Jack Fowler, Ph.D., D.Sc.¹
Thomas Rockwell Mackie, Ph.D.^{1,3,6}
Mark Ritter, M.D., Ph.D.¹
Jeff Kapatoes, Ph.D.³
Lisa Forrest, V.M.D.⁴
Richard Chappell, Ph.D.¹
Bhudatt Paliwal, Ph.D.^{1,6}
Minesh P. Mehta, M.D.¹

¹Department of Human Oncology
University of Wisconsin
Madison, Wisconsin, USA

²University of Western Ontario/
London Regional Cancer Program
London, Ontario, Canada

³TomoTherapy Inc.
Madison, Wisconsin, USA

⁴School of Veterinary Medicine
University of Wisconsin
Madison, Wisconsin, USA

⁵UW Cancer Center-Riverview
Wisconsin Rapids, Wisconsin, USA

⁶Department of Medical Physics
University of Wisconsin-Madison
Madison, Wisconsin, USA

Disclosures/Conflicts of interests:
The authors associated with Tomotherapy Incorporated have a financial interest in that company

*Corresponding Author:
James Welsh, M.S., M.D.
Email: welsh@humonc.wisc.edu

sions need to be made regarding the choice of equipment, optimization method, image feedback, organ deformation registration, and immobilization. We have identified limitations of existing IMRT systems and are attempting to address these with helical tomotherapy using online megavoltage computed tomography (MVCT) imaging, verification of patient positioning prior to and during treatment, verification of delivered dose, treatment modification to account for patient/organ displacement, and deformable reconstruction to account for organ motion and change in shape. These processes, which form the core concept of adaptive radiotherapy, allow for ongoing verification and continuous correction of treatment variations. The clinical application of these techniques opens up new clinical vistas for Radiation Oncology.

Optimized Treatment Delivery: A Description of Helical Tomotherapy

Helical tomotherapy represents a new form of radiation treatment delivery, which has been pioneered at the University of Wisconsin and is now in use at various centers around North America (2). While standard radiotherapy is currently delivered using a few static fields, helical tomotherapy delivers treatment with a rotating, intensity-modulated fan beam. The patient is continuously translated through a ring gantry resulting in a helical source trajectory about the patient. The beam delivery is similar to that of helical ("spiral") computed tomography (CT) and requires slip rings to transmit power and data. The ring gantry provides a stable and accurate platform to perform tomographic verification of both the patient setup and delivered dose.

Various systems have been developed to implement IMRT. In this regard, helical tomotherapy is most similar to the NO-MOS Peacock™ system. The Peacock™ system also uses a fan beam delivered via an arcing gantry equipped with a multileaf collimator. However, it delivers treatment by "translate-then-rotate" method rather than a continuous helical delivery because it is an attachment to a standard C-arm linear accelerator. The design of the helical tomotherapy unit allows for continuous delivery over 360 degree beam angles (3). In addition, this design minimizes the treatment time, which may hypothetically provide a radiobiologic advantage compared to other IMRT approaches (3, 4). The helical delivery minimizes the risk of significant high or low dose deposition in areas of overlap or junctioning (6). Assessments of sequential units presently in use, reveal that positioning errors as little as 1 mm can cause dose errors on the order of 10-20% in the abutment regions (7). In addition to full integration of IMRT delivery, an important advance with helical tomotherapy over the other current systems is the ability to provide accurate verification of radiation delivery via onboard tomographic imaging.

Adaptive Radiotherapy

Perhaps the most significant difference of the helical tomotherapy unit is the presence of an integrated online megavoltage CT (MVCT) unit. This permits verification of patient positioning, target tumor/organ registration to assess internal motion (including geometric shift, and shape/volume changes), and reconstruction of delivered dose. These capabilities offer the radiation oncology team the ability to verify and adjust the therapeutic plan as needed during the course of treatment. This concept is referred to as adaptive radiotherapy (8). These capabilities can be viewed as a closed-circuit loop, as illustrated in Figure 1. The integration of the MVCT and the treatment unit allows for options not possible with contemporary systems. For example, if a patient set-up is found to differ from the planned position, the current approach requires moving the patient to compensate for this positioning error. With the integrated helical unit, another option is having the patient remain in the "incorrect" position and modifying the treatment delivery. The success of the modification is independent of the extent and direction of the offsets, within certain limits (9). Our preliminary results with MVCT in both phantoms and patients confirm its utility in verification of patient position and tumor localization. These MVCT images can be obtained at radiation doses of around 2 cGy, comparable to that of diagnostic CT imaging (10, 11) and lower than reported doses from low-dose megavoltage cone beam CT (65). Other methods of onboard imaging have been developed recently and are available clinically. Our group has recently acquired cone-beam kVCT technology and we are presently comparing this to helical tomotherapy MVCT capabilities.

Delivery Modification: Dose Reconstruction

Unlike surgical oncology, where frozen section pathology allows rapid feedback, radiation oncologists are typically unable to rapidly assess and adjust their plans in light of their actual treatment. This is changing with the development of dose reconstruction tools, which offer the capability to determine the actual three-dimensional dose deposited. At the time of treatment on the tomotherapy unit, the incident energy fluence is computed from the signal detected at the exit detectors. An accurate, anatomically detailed, 3D representation of the patient is also obtained. A transfer matrix then converts this signal to incident energy fluence. In other words, the matrix allows one to infer from the signal at the detector the energy fluence issuing from the MLC. The integrated CT present in the tomotherapy unit provides details of the primary and scatter characteristics for every projection. Path-length and detector-to-patient distance are computed from the MVCT image. Leakage and transmission plus tongue and groove penumbra are also included in the calculation. The tongue-and-groove effect (TG) of the MLC leads to

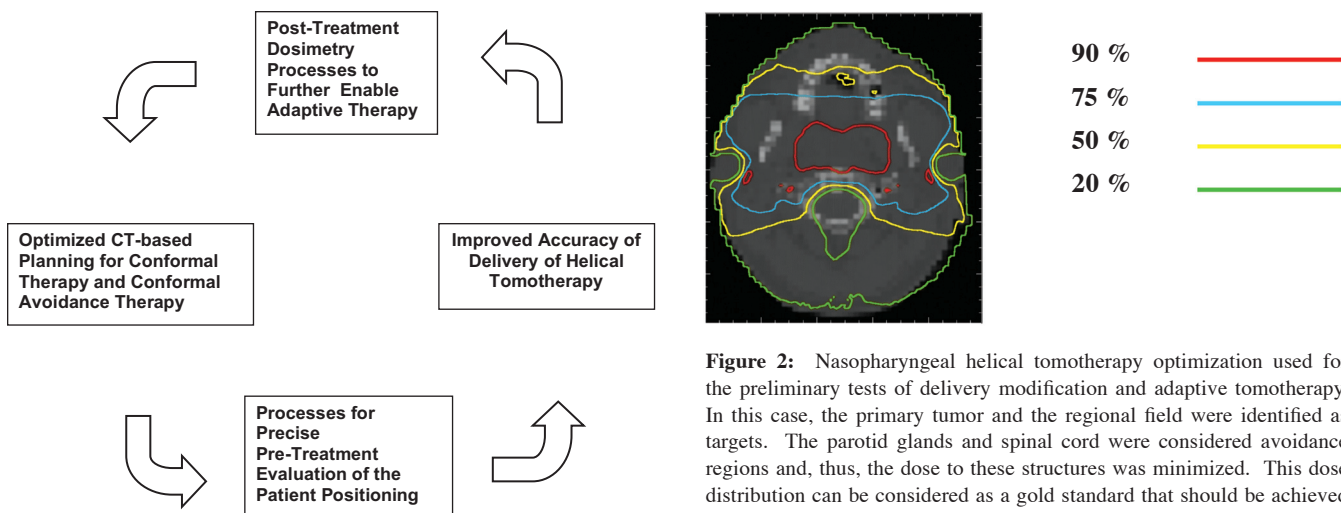


Figure 1: Conceptual Flow Diagram of Adaptive Tomotherapy. As described in the text, each clinical project within our research strategy is uniquely designed to test one or more particular component of adaptive radiotherapy.

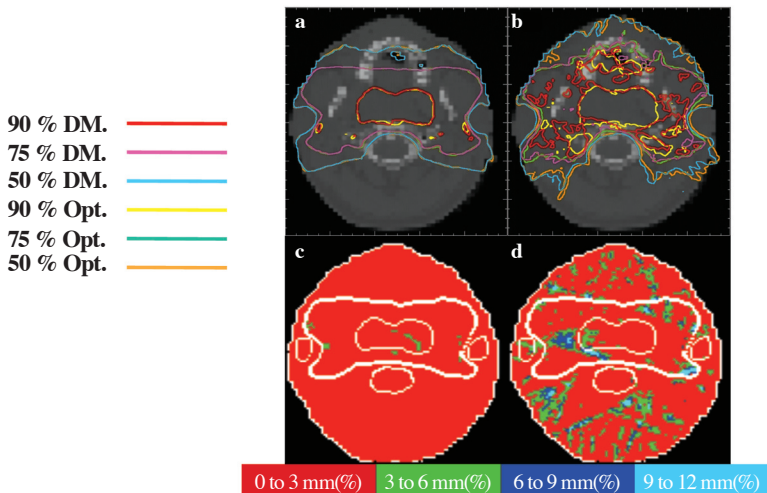


Figure 3: Examples of (a) successful and (b) unsuccessful delivery modifications following treatment given with a displacement from the intended patient position. The corresponding ξ figures are shown in (c) and (d) for the successful and unsuccessful delivery, respectively. Red indicates that the dose distributions are between 0-3% or 0-3 mm (within tolerance), green between 3-6% or 3-6 mm, blue between 6-9% or 6-9 mm, and light blue >9% or >9 mm. Very small errors can be readily identified even in the case of a good delivery-modified dose distribution (panel c). Panel d demonstrates many different levels of error present with the incorrect delivery modification. From this, it appears that the ξ distributions will be very useful to detect errors and to analyze the optimal adaptive radiotherapy approach to be pursued.

a variation in total fluence-per-leaf-opening with the number of adjacent open leaves. The planning system accounts for this effect using TG correction factors measured for each leaf. The method corrects for the limitations of other MLCs, which do not consider the latter factors, resulting in fluence errors as high as 20% in extreme situations (12). Finally, the treatment dose distribution is computed using the convolution/superposition algorithm. Kapatoes *et al.* (13) have demonstrated that the reconstructed distribution has excellent accuracy; the

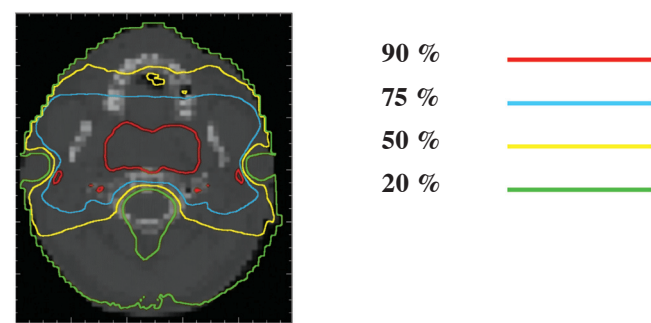


Figure 2: Nasopharyngeal helical tomotherapy optimization used for the preliminary tests of delivery modification and adaptive tomotherapy. In this case, the primary tumor and the regional field were identified as targets. The parotid glands and spinal cord were considered avoidance regions and, thus, the dose to these structures was minimized. This dose distribution can be considered as a gold standard that should be achieved during actual treatment delivery. A metric that is accurate, intuitive, simple to use, and provide quantitative and qualitative information has been developed and is called ξ that is useful in comparing three-dimensional IMRT dose distributions to this gold standard.

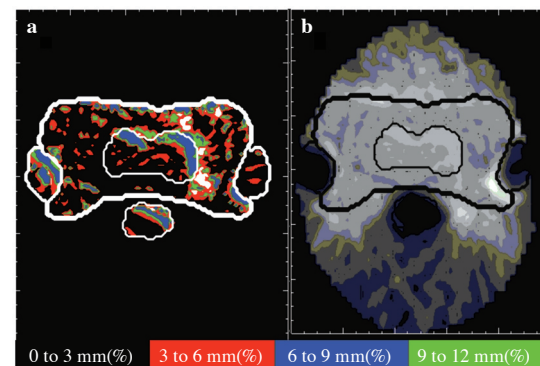


Figure 4: Example of optimization to correct for one week of incorrectly delivered dose. Panel a is a ξ image of one week's delivery with the patient shifted by 0.5 cm in the x and 0.5 cm in the y direction. Panel b is the gray scale image of the dose to be delivered in the second week designed to compensate for the previous week's error.

tolerances of the majority of voxels within the low and high dose gradient are 3% and 3 mm, respectively. Effectively this results in the generation of an accurate daily pictorial dose record, which can be fused to the treatment planning CT and compared directly with the planned dose-distribution.

Delivery Modification: Dose Comparison

The ability to accurately reconstruct the 3D dose distribution is a valuable addition to the radiation oncologist's armamentarium. However, an efficient method of comparing desired and actual dose distributions is required. An example illustrating this issue is described in Figure 2. Desired isodose lines for a nasopharyngeal cancer helical tomotherapy optimization are depicted with the parotid glands and spinal

cord areas to be avoided. This idealized dose distribution is the goal to be achieved during the actual treatment. To compare desired dose distributions with actually delivered dose distributions, a metric is required that is accurate, intuitive, easily usable, and provides the needed quantitative and qualitative information. One metric with these characteristics has been developed and is called ξ .

This method for comparing isodose distributions is based on the methods of Van Dyk *et al.* (14) and Low *et al.* (15). The two modes of comparison are dose difference (ΔD) and distance-to-agreement (DTA) analyses. For regions in which both the planned and measured distributions have high dose gradients, DTA comparisons are conducted. For all other cases, ΔD analyses are performed. Once the mode of comparison is decided, the ξ index can be computed by dividing the ΔD and DTA values by their respective tolerances:

$$\xi_{\text{high gradient voxels}} = \left| \frac{\text{DTA}}{\text{DTA tolerance}} \right|,$$

$$\xi_{\text{low gradient voxels}} = \left| \frac{\Delta D}{\Delta D \text{ tolerance}} \right|$$

The ξ value provides a measurement of quality for every voxel indicating if they are within the desired tolerance or how far they deviate from that tolerance. Typical tolerance values in IMRT are 3% and 3 mm, for ΔD and DTA, respectively. The smaller the ξ value, the more accurately the compared isodose distributions are aligned. To facilitate the spatial identification of problem areas, color-wash images of ξ maps can be displayed (Figure 3). The utility of this method is illustrated with an example below.

Delivery Modification: Examples of Adaptive Radiotherapy

Suppose that a particular patient has an offset of 1 cm in the x direction. In order to compare the optimized and delivery-modified dose distributions, the ξ metric is used. Figure 3 (panels 'a' and 'b') shows two sets of isodose lines for optimized and delivery-modified dose distributions, respectively, superimposed on the same CT image. One panel shows a successful (panel 'a') and the other an unsuccessful (panel 'b') treatment adaptation. It is quite difficult from panel 'b' to analyze precisely the impact of the delivery modification error from the isodose lines. It may be necessary to analyze many sets of isodose lines to accurately identify errors. Panels 'c' and 'd' represent the corresponding ξ distribution images for panels 'a' and 'b', respectively. In this example, red indicates that the dose distributions are between 0-3% or 0-3 mm (within tolerance), green between 3-6% or 3-6 mm, blue between 6-9% or 6-9 mm, and light blue >9% or >9 mm. Very small errors can readily be identified even in the case of a good delivery-modified dose distribution (panel 'c').

This comparative information can be obtained during a single fraction or after several fractions. Figure 4 illustrates the ξ image comparing the planned dose and the reconstructed dose for the first week of treatment in which a systematic error was made. Several error regions appear on the targets and regions at risk, mainly in the high gradient regions. Panel 4b shows a gray scale image of the re-optimized dose distribution that could be delivered during the second week of treatment in order to correct for prior misalignment. In this dose image, a pattern appears that is very similar to the ξ image. This comparison is quite intuitive and, therefore, useful for checking by visual inspection.

Figure 5 illustrates the result of treatment with one week of treatment with a systematic error followed by a second week of either the original treatment plan given accurately (Figure 5a) or a re-optimized treatment plan designed to compensate for the errors of the first week (Figure 5b). Simply repositioning the patient and accurately delivering a week of the originally designed radiation plan (Figure 5a) will dilute the error incurred during the first week but cannot fully compensate for the error. Radiation delivery modifications are designed to compensate for the difference between actual and desired dose distributions. In the example presented, dose reconstruction and comparison reveal that excess dose is being deposited in the spinal cord and right parotid. In Figure 5b a modified plan specifically designed to compensate for the errors of week one is instituted in the second week and the dose reconstruction is performed again. Figure 5b shows the ξ image comparing the reconstructed dose delivery after two weeks of the incorrect and corrected treatments. Most of the errors within the tumor region are corrected. However, a small trade-off with dose to the parotid glands and spinal cord is necessary in order to rectify the errors induced during the first week of delivery. The specific thresholds for the trade-offs that should be accepted remain a matter of ongoing physics and clinical research.

With helical tomotherapy, MVCT images can be registered using a full mutual information algorithm, bone extracted feature fusion (EFF), and bone and tissue EFF algorithms, with uniform down-sampling of the MVCT images along the x and z axes (to provide a time-saving by a factor of up to 4) with and without the rotational registration components. These particular algorithms take into account any changes in patient anatomy between the reference image and fusion image when the image registration is carried out.

Conformal Avoidance IMRT

Current Paradigm & Pitfalls of Wide-Field Irradiation

A critical element in improving the therapeutic ratio in radiotherapy is the minimization of normal tissue irradiation. In

many clinical situations, the difficulty in precisely identifying specific regions at risk for tumor invasion has led to the default paradigm of “wide field irradiation” to include potential cancer-bearing sites with confidence. Clinical examples of this abound, and the treatment of head and neck cancer provides an instructive example.

Current Head and Neck IMRT Paradigm for Xerostomia

One of the more popular clinical applications of IMRT in the context of normal tissue sparing involves avoidance of major salivary glands during head and neck radiotherapy. Xerostomia, with its consequential taste impairment, difficulty chewing, speaking and swallowing, and increased dental caries and oral candidiasis, is a common toxicity experienced by head and neck cancer patients undergoing radiotherapy. These chronic complications represent a major source of quality of life deterioration for survivors, with nasopharyngeal cancer patients often experiencing notable effects due to the large volume radiation fields commonly employed (16).

Temporary symptomatic relief offered by moistening agents and saliva substitutes represents the only viable option for patients without residual salivary function. In patients with some residual salivary function, selected studies demonstrate that oral administration of pilocarpine can increase salivary flow and ameliorate symptoms (17) while other studies have contradicted these findings (18). The effectiveness of muscarinic cholinergic receptor agonists requires residual salivary function, which emphasizes the importance of sparing normal salivary tissue during irradiation (19). Based on a Phase III randomized trial, amifostine was approved for xerostomia prevention in the postoperative head and neck cancer setting. The incidence of clinically significant xerostomia was 57% in the control group and 34% in the study group ($p = 0.002$). Although statistically significant, this implies an overall absolute gain of only 23% (20).

Scintigraphic evaluation of post-radiation parotid function suggests that when bilateral whole parotid glands are irradiated, partial recovery is possible if the dose to the parotid is less than 52 Gy; however, recovery rarely occurs at doses exceeding 55 Gy. The 50% complication probability dose is less than 33 Gy for subacute xerostomia (<6 months) and 52.5 Gy for chronic xerostomia (>12 months) (21).

Eisbruch *et al.* (22) reported results using salivary gland sparing techniques. Forty-eight patients with unilateral treatments served as a comparison group. Treated parotid glands received an average dose of 55.2 Gy, while spared glands received 21.9 Gy. Unstimulated and stimulated parotid flow rates decreased dramatically in treated glands after the initiation of radiotherapy, remained low without detectable improvement, and were significantly lower at two years after

radiotherapy compared with baseline. Conversely, parotid flow rates in spared glands underwent mild changes during radiotherapy and returned to baseline values at two years. Patients who had undergone unilateral treatment demonstrated a compensatory increase in salivary production by the spared glands. These results suggest that using conformal techniques to spare the parotids can enable meaningful improvement in xerostomia over time. Butler *et al.* (23) reported an attempt to minimize xerostomia using IMRT boost techniques. The mean dose delivered to the ipsilateral parotid was 23 Gy, and the contralateral parotid received 21 Gy; these mean doses were a function of a planned delivery of 50 Gy to the neck nodal regions. Often 60–70 Gy is required in these situations, and even with IMRT, the parotid dose may exceed the 50% tolerance dose of 33 Gy for subacute xerostomia. Although these studies are promising, they suggest that even with conventional IMRT, there is considerable room for improvement in parotid gland protection.

Conformal Avoidance: A New Paradigm Applied to Xerostomia

The current IMRT paradigm requires the clear delineation of target regions and organs at risk (24, 25). This paradigm requires meticulous and labor-intensive contouring of the target volume and at-risk lymph node regions. In addition, there remains a risk for geographic miss and consequential nodal failure. Due to the inability to precisely define and map tumor regions along with the need to prophylactically address nodal regions, large volumes of normal tissues are commonly still irradiated despite IMRT techniques (26). The concerns regarding geographic miss may result in mapping a larger region than necessary; thereby, eroding the advantages of IMRT dose conformality. The counterpart to this paradigm of target mapping is *conformal avoidance* (27). This strategy may prove easier to execute routinely than conformal targeting. It is anticipated that the routine definition and mapping of normal tissue structures in the head and neck (*i.e.*, parotid glands, eyes, spinal cord, mandible) can be accomplished with greater ease, precision, and reproducibility across users than the process of delineating primary tumors with infiltrative soft tissue extension and associated regions of nodal spread as currently required for IMRT techniques. Conformal avoidance may offer the oncology team greater confidence that cancer-bearing regions will receive full dose radiation while defined normal tissues are specifically avoided (Figure 6).

Testing Conformal Avoidance with Helical Tomotherapy

With the conformal avoidance approach, it may be possible to spare both parotid glands in addition to other normal head and neck tissues. Therefore, one of the major hypotheses to be tested with helical tomotherapy is its capacity for conformal avoidance in situations where normal tissues are in close

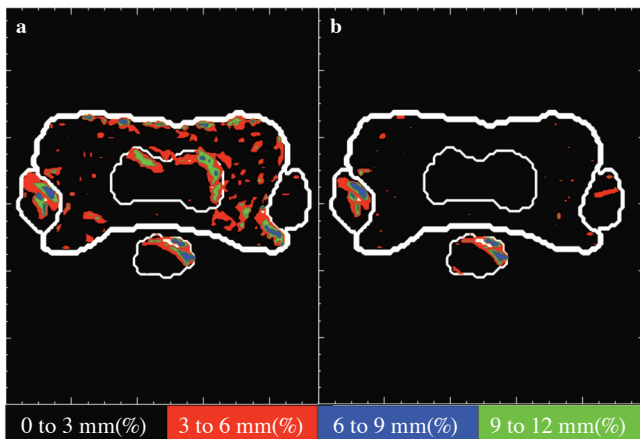


Figure 5: Panel a compares the ξ image after the second week if no action is taken to correct for errors during the first week. Panel b shows the ξ image if action is taken to correct for the error.

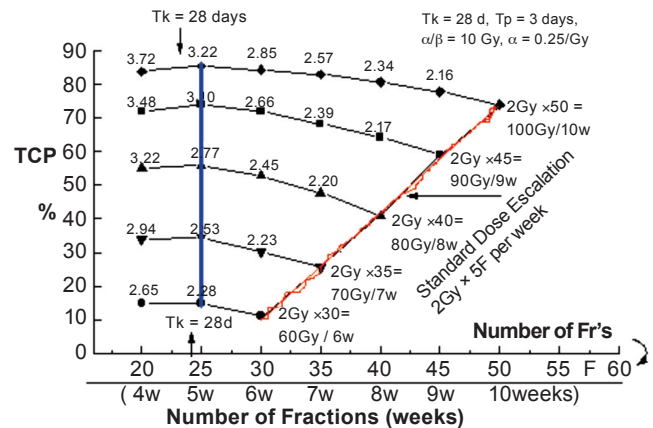


Figure 7: Dose escalation for NSCLC can take several paths. The conventional strategy of adding more fractions of 2 Gy each is shown on the right in red. Another approach is to increase the size of each fraction and simultaneously shorten the time of the overall course to five weeks to account for tumor cell proliferation (blue line). Tk, the point at which cell proliferation accelerated is, assumed to be 28 days in this model.

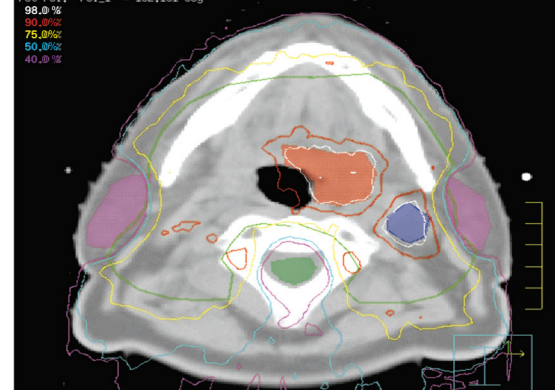
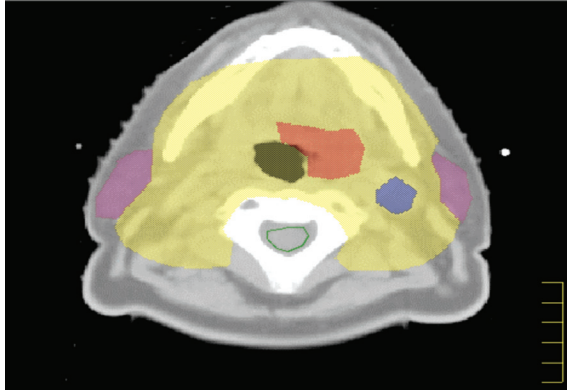


Figure 6: Conformal avoidance tomotherapy. The tumor target (red) and the grossly involved node (blue) are contoured and planned for high-dose conformal therapy whereas the parotids (purple) are simultaneously conformally avoided.

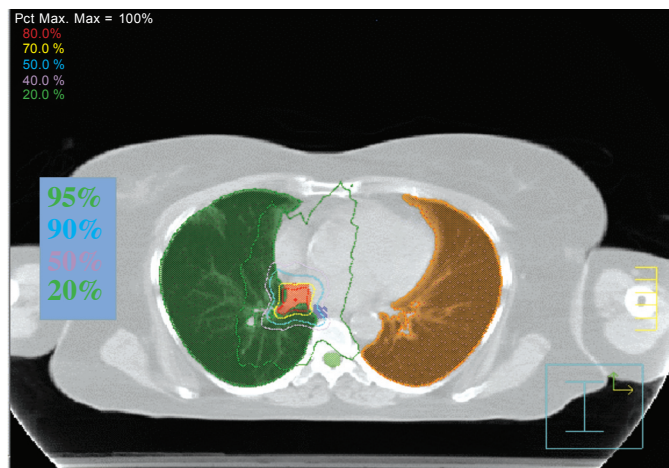


Figure 8: An example of conformal helical tomotherapy for NSCLC demonstrating the ability to effectively target areas of disease while simultaneously minimizing dose to normal lung. Such dose distributions may allow clinical implementation of dose-fractionation schemes previously considered impractical or risky.

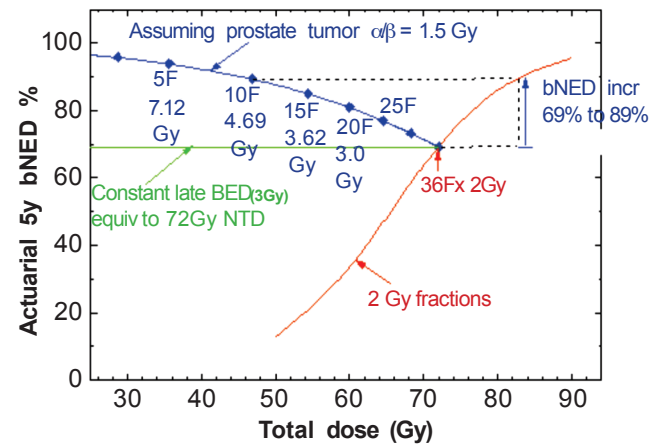


Figure 9: Using ten fractions of 4.7 Gy should yield the same late complication probability but increased bNED (biochemical no evidence of disease) as if 72 Gy were increased to 83 Gy in 2 Gy fractions, assuming an α/β ratio of 1.5.

proximity to tumor-bearing regions. Various elements of conformal avoidance are being tested and developed in ongoing clinical projects; the first study is a veterinary trial of canine patients with nasopharyngeal tumors. Radiation therapy is the standard treatment for dogs with spontaneously occurring nasopharyngeal tumors but ocular toxicity is a common consequence due to the anatomy of the canine head where the nasal cavity and sinuses extend to and beyond the level of the eyes. Therefore, at least one eye receives a large percentage of the total dose using conventional treatment planning. Experience suggests a substantial rate of ocular and visual toxicities, which can be severe in these dogs. In a study of 21 dogs with malignant nasal tumors treated conventionally with 42 Gy in ten fractions, acute ocular toxicity was noted in 95%. Late ocular effects included progressive cataracts, radiation retinopathy, and keratoconjunctivitis sicca. Degenerative ocular changes progressed to blindness in 12 of 28 eyes evaluated and three dogs developed bilateral blindness (28). These toxicities are readily measurable and are almost universal in incidence; therefore, the canine nasopharyngeal tumor presents an ideal model to assess the ability to conformally avoid critical structures in a small, yet appropriately powered sample. Intracavitary dosimeter measurements are easily conducted on the anesthetized animals allowing the dose to be verified experimentally as well as calculated through MVCT based dose reconstruction. The experience gained in treating these animals will form the basis for extending the clinical application of helical tomotherapy in human trials. Preliminary results demonstrate effective treatment of the primary tumors with minimal early ocular toxicity (29).

The clinical implementation of head and neck helical tomotherapy in human trials will proceed in a careful stepwise fashion. We are currently gaining experience in conformal avoidance treatment planning by designing tomotherapy plans for patients undergoing conventional head and neck cancer radiotherapy and who are considered to be at significant risk of xerostomia (more than 75% of bilateral parotid glands receiving > 45 Gy). These patients will undergo planning CT simulation, and treatment plans will be developed on our standard 3D treatment planning software (Pinnacle). Plans will also be developed for optimized helical tomotherapy. Patients will undergo baseline toxicity analysis including salivary measurements, audiometric and otoacoustic testing, swallow function evaluation, and quality of life analysis in the pre- and post-treatment setting. Data from this cohort will provide baseline data from our institution regarding toxicity rates for comparison with future head and neck tomotherapy treatments.

In the second phase of our head and neck tomotherapy clinical implementation, a cohort of patients will be planned and actually treated using helical tomotherapy. The primary objectives of this phase include: a) safety confirmation of tomotherapy treatment delivery with inclusion of comprehensive *in vivo* dosimetry and monitoring of patient outcome and b) further testing for one of the key processes in helical tomotherapy of particular relevance in head and neck cancer, namely set-up verification. As in the preclinical phase described above, patient toxicity will be monitored *via* measurement of salivary output, audiometric, otoacoustic, and swallowing assessment as well as quality of life surveys specific to head and neck cancer patients. This study will also test the MVCT capacity of the helical tomotherapy system to detect a patient's position on a given day, relative to their position at the time of their planning CT scan. Patients will be set up for treatment using standard head and neck immobilization techniques (custom face mask affixed to the head and neck base plate). We will then determine daily set up variation using MVCT and an infrared radiocamera system (SonArray™, ZMed, Inc., Ashland, MA) that has been tested and confirmed accurate to within 0.2 mm (see section on *Optical Guidance* below). This will serve as the "standard" against which the tomotherapy MVCT registration system will be tested. Each patient's displacement/rotation will be measured prior to treatment once per week using both systems to allow the accuracy of the setup verification system to be established.

In the third phase of the head and neck tomotherapy clinical implementation process, a clinical trial will be carried out in which advanced head and neck cancer patients are treated with helical tomotherapy. This trial is designed to examine the capacity of conformal avoidance tomotherapy to improve functional outcome in head and neck cancer patients *via* selective sparing of salivary glands, and auditory apparatus. Objective data will be accrued for salivary, auditory and swallow function endpoints. Similarly, validated quality of life instruments will be used for all head and neck tomotherapy patients. Additionally, the processes of setup verification and subsequent treatment modification (*i.e.*, adaptive radiotherapy) for head and neck cancer patients will be further tested.

The ultimate goal of the clinical implementation of head and neck helical tomotherapy is to improve quality of life for advanced head and neck cancer patients while maintaining equivalent or increased cure rates. Both the canine and human studies will require specific capabilities for successful implementation. In particular, these two projects will be enhanced by the ability of helical tomotherapy to detect set-up error, provide data to rectify error, and to generate plans compensating for set-up errors using treatment modification parameters. Some degree of set-up error and organ motion is unavoidable. The magnitude of these uncertainties for specific sites, and for various set-up techniques, has been quantified in the literature. Booth and Zaygorodni (30) have tabulated the impact of these factors in head and neck cancer radiotherapy, and their data suggests that the best current immobilization and verification systems still have a day-to-day

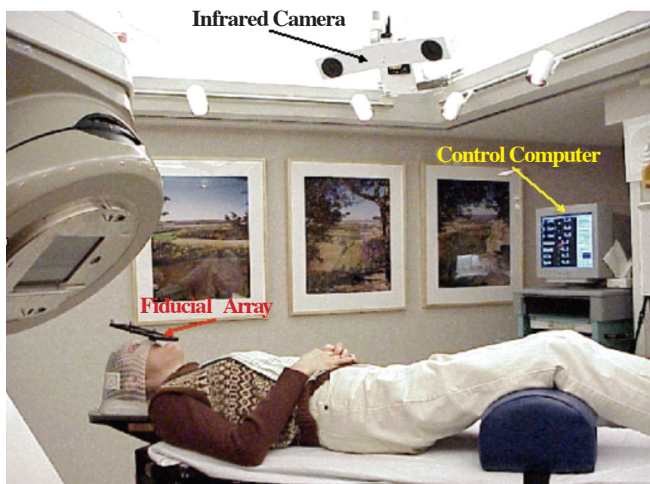


Figure 10: In this optically guided FSRT/IMRT system, localization is separated from immobilization through detection of four passive markers that are attached to a custom bite plate to form a rigid system. Translations and rotations are tracked in real time using an optical position sensor system mounted to the ceiling and interfaced with the computer. Definition of treatment room stereotactic space relative to the linac isocenter is accomplished using a rigid body calibration apparatus equipped with passive markers that have known locations. The calibration apparatus is precisely positioned relative to the isocenter using a stereotactic floor stand. After calibration, the position of any passive marker in the room may be defined relative to a calibration matrix. Since three points define a plane, any three passive markers in a fixed relationship may be used to define the rotational and translational characteristics of the rigid body relative to this defined virtual space. This system allows one to localize patients between fractions in the treatment room within 0.3 mm-translation error and 0.3 degrees of rotation error.

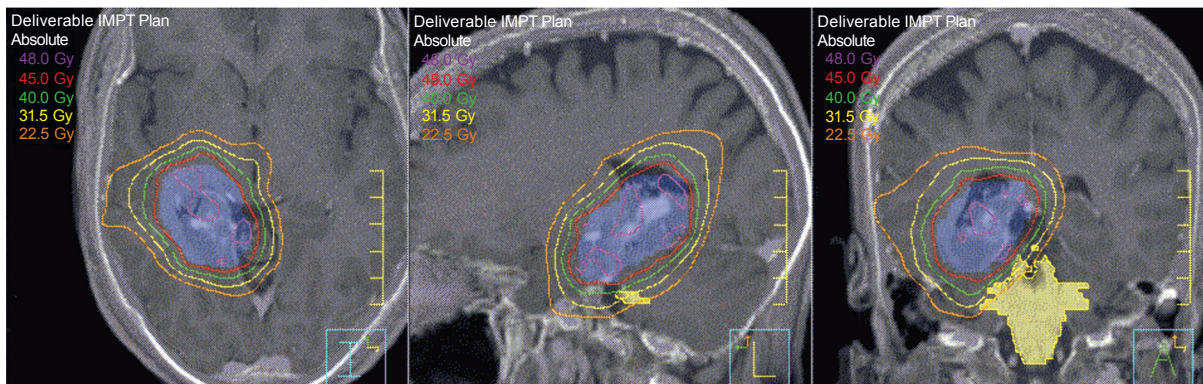


Figure 11: This pilocytic astrocytoma was treated to a total dose of 45 Gy and treatment planning was performed using three approaches: a standard 3-field, an FSRT, and an helical tomotherapy IMRT approach; the resulting dose-distributions are presented as dose-volume histograms in Figure 12. The tomotherapy plan results in the greatest sparing of normal brain tissue as demonstrated by the PITV values are 3.16, 1.65, and 1.45, for the 3-field conventional, 3-D FSRT, and helical tomotherapy plans, respectively.

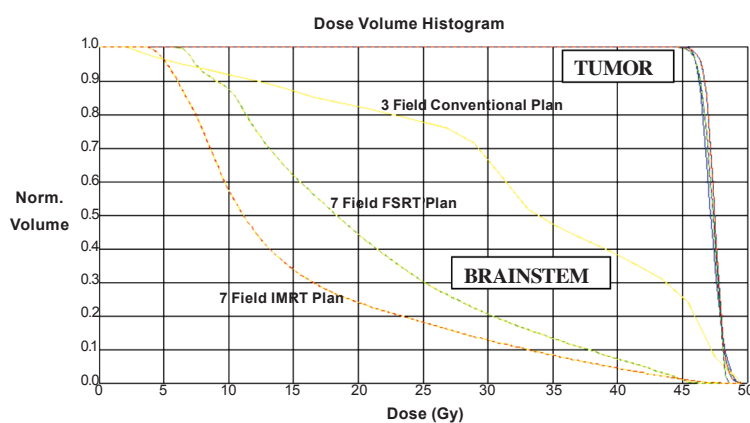


Figure 12: DVH comparisons of the various techniques illustrated in Figure 11. The tumor DVHs are illustrated by the three curves in the upper right corner, which demonstrates that the entire tumor receives at least 45 Gy with small proportions up to 49 Gy. Tumor coverage is virtually identical with all techniques. The dose to the brainstem, however, is considerably different. The dose received by 50% of the brainstem is 34 Gy, 17 and 12 Gy with the 3-field, FSRT, and helical tomotherapy methods respectively.

error of 4-8 mm. Accounting for such errors in two directions would require field expansion of 8 to 16 mm, which could negate the potential benefits of conformal avoidance. Therefore, the inherent verification and modification capabilities of helical tomotherapy will be necessary to achieve the promise of conformal radiotherapy.

Our early results demonstrate that conformal avoidance radiotherapy using helical tomotherapy for head and neck cancers as well as other disease sites can be effectively achieved and the goals stated above can be fully realized. The early veterinary experience has shown that spontaneous canine nasopharyngeal tumors can be effectively irradiated without excessive ocular toxicity despite the proximity to the eyes (29). In dosimetric comparisons to other techniques, helical tomotherapy appears to be able to provide superior radiation dose distributions for total or partial scalp irradiation, while avoiding the underlying brain

and nearby eyes (66, 67). In a non-head and neck example, further evidence that exquisite conformal avoidance is possible with helical tomotherapy was provided by a study that demonstrated the feasibility of delivering total body or total marrow irradiation while minimizing non-target tissue dose (68). A final example which clearly suggests the potential of helical tomotherapy conformal avoidance is provided by the creation of a dosimetrically equivalent “mantle”. This study showed that one could reproduce the same desirable radiation doses to at-risk nodal areas that are achieved with the mantle field, while sparing the sensitive normal structures of the high dose that has caused the old (but effective) mantle field technique to fall out of favor (68).

Conformal Dose-per-fraction Escalation

Once the adaptive radiotherapy, conformal avoidance, and immobilization potentials described above are evaluated and verified, the next logical step will be to adjust dose delivery to improve local control and possibly increase survival rates. The rationale for the helical tomotherapy dose-fractionation regimens contemplated at our institution is discussed below.

Improved Local control Improves Survival

The cure of several major cancers is constrained by two equally important processes: loco-regional failure and distant spread. In situations where metastases have not yet occurred, improved loco-regional control has the potential to yield improved survival. In an attempt to improve local control in non-small cell lung cancer (NSCLC), efforts to escalate dose have achieved doses of 80-100 Gy, but prolonged over courses of ten weeks (31). Although control was improved, these trials have not yielded the expected gains, perhaps because of this prolongation.

Two opposing forces are at play in prolonged fractionation schedules: clonogenic death due to the increased radiation dose and accelerated repopulation that is not adequately overcome by the increase in dose. For tumors with short potential doubling times, it may be wiser to deliver the required extra radiation dose as an increase in dose-per-fraction rather than an increase in the number of fractions (32). A secondary negative impact of the prolonged treatment schedules is the psychological and economic hardship imposed on patients and society by committing a substantially greater proportion of time to therapy. In the United States, a major driver for radiotherapy cost is the duration of treatment. A schedule increase from six to ten weeks can result in a 40-50% increase in the overall cost of radiotherapy for that particular disease process (33, 34). Based on this information, our dose escalation strategy using helical tomotherapy for non-small cell lung cancer (NSCLC) is focused on shortening the overall treatment schedule and increasing fraction size. A higher

biologically equivalent dose (BED) can be achieved with unprecedented precision; thereby, avoiding the previously obligatory increase in late complications.

Developing dose-per-fraction escalation protocols is impractical without knowledge of specific radiobiologic parameters. Until recently, the proliferation rate of NSCLC was not well characterized. Fowler *et al.* (35) analyzed data on 397 lung tumor patients treated on an RTOG study reported by Cox *et al.* (36). Seventy patients who experienced treatment delays of five or more days were observed to have 1- and 3-year survival probabilities of 37% and 1%, versus 56% and 17% in patients without treatment delays. The median loss in survival probability was calculated to be 1.6% per day of prolongation beyond six weeks, the same rate as previously accepted in head and neck tumors. This rate of loss of tumor control with treatment prolongation corresponds to a clonogenic doubling time of 3 to 3.5 days. It is evident from such data that NSCLC is a rapidly proliferating tumor that may not benefit from prolonged dose-escalated treatment schedules and we have used this information for modeling our helical tomotherapy schedules for NSCLC.

Our strategy is to first test an accelerated fractionation schedule with linac-based IMRT and then further increase total dose by escalating the daily fraction size. In the case of NSCLC, our modeling data suggest that the optimal treatment duration is approximately five weeks. We anticipate pneumonitis to be the rate limiting toxicity. Therefore, patients will be stratified into five classes based on the volume of lung irradiated, analogous to the strategy developed by the University of Michigan (37). In this trial, we will also compare two separate binning methods: V20 and mean normal tissue dose (NTDmean).

Further Rationale for Increasing BED by Increasing Fraction Size

The biological rationale for increasing fraction sizes in the present lung dose escalation proposal has been previously outlined (38). It was shown that for constant late complications, as fewer and larger fractions are used, the optimum overall time (measured in weeks) is slightly longer than the tumor cell doubling time (measured in days). This optimum occurs because of two conflicting trends as fewer fractions are used. First, the tumor control probability (TCP) *increases* because of the avoidance of accelerated proliferation with the shorter overall times. However, TCP may also *decrease* because total dose must be reduced to avoid increased complications. Both trends can be modeled; the first, if we know the tumor proliferation rate, and the second if we know the α/β ratio for the late complications. Figure 7 illustrates the optimum TCP predicted for NSCLC from our modeling. Figure 7 illustrates the consequences of one further assumption:

tion, the starting time, T_k , of the accelerated proliferation. The optimum TCP cannot occur at courses shorter than T_k . T_k has been controversially discussed as possibly between 14 and 32 days, but statistical analysis of clinical data has favored rather long times for T_k , with 28 days representing a conservatively long consensus (39-41). Since the optimum TCP occurs at slightly longer time than T_k , we do not propose to shorten to less than five weeks in the present study.

Helical Tomotherapy Treatment Planning: NSCLC Example

For this dose escalation strategy to be successful, helical tomotherapy will have to be utilized not only to produce conformal dose distribution around a well-defined tumor, but also to minimize the volume of normal lung irradiated to high dose. To test the conformal capabilities of helical tomotherapy, several patients with NSCLC were planned for simulated tomotherapy treatment and compared to the actual treatments, which consisted of a standard 2-phase approach, with parallel-opposed AP-PA beams followed by an oblique pair boost. Helical tomotherapy planning uses the convolution/superposition dose-calculation method, which is capable of accurately modeling the penumbra blurring and reduced photon attenuation in lung tissue. The resultant dose distributions are highly conformal and permit very sharp dose gradients around the tumor volume. Compared to the conventional treatment plans, there is more homogeneous coverage of the target volume and lower doses delivered to the normal lung parenchyma, esophagus, and spinal cord (Figure 8). These improvements in normal tissue sparing and improved target coverage, when combined with verification processes to prevent geographic miss, should allow dose escalation beyond what is possible with traditional 3-D techniques.

In a separate study, five patients with inoperable stage III NSCLC were formally studied, representing a variety of tumor sizes and locations (42). For each patient, two treatment plans were generated: one using optimized 3D treatment planning techniques and one using helical tomotherapy. Normal tissue V20, NTDmean, and effective uniform dose (EUD) for a given tumor dose were compared and tumor doses possible for a given mean normalized lung dose were also computed and compared. In order to obtain a meaningful comparison, the helical tomotherapy plan was optimized with the objective of minimizing normal tissue doses as much as possible while using an equivalent planning target volume dose as the 3D plan. The lung doses were significantly lower with helical tomotherapy in all five cases. For the lungs taken together as a single organ, the mean normalized doses with tomotherapy planning ranged from 2.05 Gy to 8.36 Gy (mean 5.7 Gy), versus 4.4 Gy to 13.62 Gy (mean 8.1 Gy) with 3D planning. The V20 for both lungs was also lower in each case with helical tomotherapy. On average, for both lungs, helical tomotherapy allowed a 22% reduction

in V20 and a 30% reduction in NTD mean when compared to 3D planning. The mean spinal cord dose was also markedly lower with helical tomotherapy. Based on these data we conducted a virtual dose-escalation trial and concluded that helical tomotherapy has the potential to significantly decrease radiation dose to lung and other normal structures in the treatment of NSCLC. This has important implications for dose escalation strategies in the future.

Increasing BED by Dose-per-Fraction Escalation: Prostate Cancer

The BED-dose escalation strategy will also be tested for prostate cancer. Retrospective studies have indicated a substantial dose response for prostate cancer. Hanks *et al.* examined Patterns of Care data and found actuarial local recurrence rates of 37% for T3 patients treated to less than 60 Gy, 36% for doses of between 60-64.9 Gy, 28% for 65-69.9 Gy, and 19% for doses of 70 Gy or more (43). Similarly, Perez *et al.* found 38% local recurrences for doses less than 60 Gy, 20% for doses between 60, and 70 Gy and only 12% for doses of 70 Gy or greater (44). A randomized trial has confirmed superior PSA recurrence-free survival when greater than 70 Gy was delivered, for intermediate or higher risk patients (45). These results provide a strong rationale for the delivery of higher than conventional radiation doses. When delivered with conventional techniques, however, doses higher than 70 Gy are associated with higher complication risks (46). It has now become clear that 3D conformal radiotherapy demonstrates better than historically expected tolerance of normal tissues to higher doses, but complication rates, particular rectal bleeding, can still be substantial (47). Various analyses suggest that the total area of rectal wall exposed to greater than 60 or 70 Gy predicts the rate of rectal bleeding. Therefore, the implementation of IMRT, with its ability to reduce rectal irradiation, can reduce toxicities (48). Such IMRT strategies are compromised by prolonged schedules and higher costs. Therefore, analogous to our NSCLC approach but for different radiobiological rationale, we plan to evaluate dose-per-fraction escalation, maintaining a constant schedule length and utilizing fewer fractions.

The radiobiological basis for utilizing this option in prostate cancer is its uniquely slow proliferation rate compared with other tumor types. The labeling indices (LI) for prostate cancer are extraordinarily low, with most reports suggesting levels below 1%, and a median T_{pot} value of 40 days (range 15 to 170) (49). Recent suggestions have also been made that the α/β ratio of prostate cancer may be remarkably small (even smaller than 3 Gy, the α/β ratio for many late responding tissues), far below the classic α/β ratios of around 10 for rapidly proliferating neoplasms. Brenner and Hall (50) investigated whether current fractionation schema for the treatment of prostate cancer with radiation could be improved; they ana-

lyzed two data sets, one using external radiation and the other permanent seed implants, using the linear-quadratic model for analysis. Their results suggest that prostate cancer may be significantly sensitive to changes in fraction size. They estimated an α/β value of 1.5 (95% CI = 0.8, 2.2), and concluded that external beam radiotherapy for prostate cancer should be designed using larger doses per fraction. We (51) have evaluated additional patient datasets from 1400 patients from 13 centers and confirmed the conclusion that α/β is as low as 1.5 with a narrower 95% confidence range of 1.2-1.8 Gy. Brenner *et al.* (52) have derived a value of α/β = 1.2 Gy from clinical hypofractionated boost data, although with only 121 patients and a rather short follow-up. Duchesne and Peters (53) have also argued in favor of hypofractionated boosting. Assuming these low α/β estimates, hypofractionation schemes could be designed that would be expected to maintain current levels of tumor control while reducing late sequelae or alternatively, increasing tumor control while maintaining a constant level of late complications. Either approach would provide the logistic and financial advantages of fewer numbers of fractions. We, therefore, propose in Figure 9 that dose escalation studies in prostate cancer should not be achieved by simply increasing numbers of 2 Gy fractions (red line in Figure 9) but instead utilize hypofractionated schedules as indicated in the curves (blue line) rising to the left. This would reduce the numbers of fractions required from around 40 to roughly half that many using daily fractions of 2.5-3 Gy. With further experience, even fewer and larger fractions could be used, with appropriate reduction in total dose, to obtain greater tumor control at the same risk of late complications. This regimen can best be achieved in the context of minimizing the volume of rectal mucosa, and bladder volume exposed to these large fraction sizes. The key focus of research in this study will be safe dose-escalation, using both the rectal balloon technique (54) and conformal avoidance to minimize the volume of rectal mucosa irradiated. While strategies involving biological dose escalation *via* an increase in dose per fraction are certainly not limited to helical tomotherapy, in our investigations, the exquisite conformal avoidance capabilities of helical tomotherapy will undoubtedly be helpful in permitting the delivery of the large fractions to well-defined prostate volumes and simultaneously avoiding high doses to the rectal mucosa.

Finally, with helical tomotherapy the larger fractions should not take longer than conventional radiation therapy and may actually be considerably quicker than other forms of IMRT such as "step and shoot" segmental IMRT and serial tomotherapy. As mentioned earlier this may be advantageous, especially for prostate cancer with its low α/β ratio (4, 5).

IMRT: The Problem Of Motion

Many IMRT approaches rely on increasing the number of beam directions and in modulating beam intensity such that

there is consequential creation of multiple tiny sub-beams. While this improves dose-distributions, the clinical applicability of such tiny sub-beams requires immense precision; the slightest patient/organ/tumor motion is likely to result in unintended dose deposition. Therefore, although fantastic dose-distributions and DVHs can be created, their clinical application must be approached with caution. Many patient immobilization systems have evolved to address this issue.

Optical Guidance

Non-invasive head frame systems often rely on external contours of the head and face, and have immobilization errors of 2-4 mm in favorable circumstances. Such systems include the Heidelberg system, which has a reported accuracy of 2 mm (55), the Laitinen's stereoreader with a measured error of approximately 2 to 3 mm (56), and the Gill-Thomas-Cosman, which uses a maxillary bite block system to yield reproducible immobilization and repeat fixation (57) and a reported accuracy of 0.5 to 1 mm. The optically guided FSRT/IMRT approach in use at the University of Wisconsin is a non-invasive system (Figure 10) where localization is separated from immobilization. This is accomplished through detection of four markers attached to a custom rigid bite plate. The location of these markers in space (tracked relative to the isocenter) is accomplished in real time using an optical position sensor system mounted to the ceiling of the accelerator vault and interfaced with a computer. The interfraction translational error and rotational error is within 0.3 mm and 0.3 degrees, respectively. Tomé *et al.* (58) have shown that this optically guided system, in conjunction with IMRT planning, allows the generation of highly conformal treatment plans that exhibit smaller 90%, 70%, and 50% prescription isodose volumes, improved PITV ratios (the ratio of the prescription isodose volume to tumor volume), comparable or improved effective uniform dose (EUD), smaller NTD_{mean} for critical structures, and an inhomogeneity index that is within generally accepted limits. In addition, optically guided treatments allow real-time monitoring of treatment delivery, providing further confidence in the patient's actual delivered dose distribution. For helical tomotherapy, such optical guidance will be useful in verifying that the patient has not moved between MVCT and treatment.

To demonstrate the clinical relevance, an early implementation of this system is illustrated in Figures 11 and 12. This patient with an astrocytoma required radiotherapy and was planned with 3-D conformal techniques, multi-non-coplanar field FSRT, and IMRT. In all three treatment planning scenarios, CT-MR fusion was utilized and the defined GTV/CTV was constant. A mathematical descriptor, PITV (the ratio of the prescription isodose volume to tumor volume) is frequently employed to evaluate dose-conformality. The ideal PITV ratio is 1; values up to 2 are commensurate with good

stereotactic radiosurgery plans. In the example presented in Figure 11, the PITV values are 3.16, 1.65, and 1.45, for the 3-field conventional, 3-D FSRT and helical tomotherapy plans, respectively. The DVHs in Figure 12 reveal substantial improvement in brain stem dose reduction as the technical approach becomes more sophisticated. The superior patient immobilization, day-to-day alignment and position-verification afforded by the FSRT and the IMRT systems using an optically guided system, allowed for a substantial reduction in the PTV margins (59). This margin reduction alone can have a significant impact in improving the DVH. The conformality afforded by FSRT and IMRT lead to dosimetric improvement that might be further improved using helical tomotherapy techniques. The application of immobilization devices is practical, and the incorporation of optical-guidance provides a high degree of reliability in terms of daily positional reproducibility and for monitoring intra-treatment motion, potentially maximizing the inherent benefits of helical tomotherapy.

Ultrasound Guidance

The system described above works well as long as the rigid body approximation holds, as is the case for intracranial lesions. However, outside the cranium, soft-tissue targets can move relative to rigid fixation points (*e.g.*, bony structures) between the times of image acquisition, treatment planning, and treatment delivery. Real time imaging is useful in determining target location at the time of treatment delivery. A system based on 3D-ultrasound guidance (SonArray™, ZMed, Inc., Ashland, MA) can be used to correct for these misalignments at the time of treatment. Ultrasound is chosen because it is a flexible and inexpensive imaging modality that can easily be adapted for use in a radiation therapy treatment room. The interpretation of two-dimensional ultrasound images can be challenging and is highly dependent on the skill of the operator in manipulating the transducer and mentally transforming the 2D images into a 3D structure. Three-dimensional ultrasound imaging overcomes this limitation. The 3D ultrasound data sets are generated through optical tracking of free-hand acquired 2D ultrasound images. The position and angulation of the ultrasound probe are determined using an array of four infrared light-emitting diodes (IRLEDs) attached to the probe. An infrared camera is used to determine the positions of the IRLEDs, and this information is input to the computer workstation. The position of each image plane can therefore be determined using the IRLEDs, and an ultrasound volume can be reconstructed by coupling the position information with the images.

In addition to building the 3D image volume, optical guidance is used to determine the absolute position of the ultrasound image volume in the treatment room coordinate system. Because the relative positions of the 3D-image volume and the ultrasound are fixed, knowledge of the probe position

in the treatment room coordinate system at the time of image acquisition is sufficient to determine the position of the image volume relative to the linac isocenter. The image to probe relationship is determined by a calibration step performed at the time of system installation (60). In this way, ultrasound guidance will allow greater accuracy of treatment delivery via helical tomotherapy to various extracranial sites.

Currently, ultrasound is being used in conjunction with MVCT. We are presently conducting a comparison of ultrasound versus MVCT. Ultimately, it may be that MVCT alone will be the only image-guidance necessary.

Respiratory Gating

Two strategies have emerged to deal with the problem of respiratory motion. One strategy is to ‘immobilize’ the lung during one phase of respiration and to gate radiation to this phase. This requires the ability of patients to breath-hold for a short period of time, which may be difficult in patients with respiratory cancers. The second strategy is to radiate at a predetermined period during respiration using dynamic aperture tracking. On-line verification of the correct phase of respiration requires a respiratory monitoring device (61). Another option provided by the helical tomotherapy unit is to determine the phase of respiration using the MVCT. Individual patient respiratory patterns will be assessed during planning and an MVCT can be performed at each treatment. The treatment will then be gated to the predicted respiratory phase with the appropriate dosimetric plan.

Consequences Of ‘Hot’ And ‘Cold’ Spots

In order to irradiate in a highly conformal manner, linac-based IMRT often [but not always (70)] results in significant dose variation within target volumes. While helical tomotherapy appears to be highly capable of providing homogeneous dose distributions within targeted regions, in some situations dose heterogeneity might be advantageous. Tomé and Fowler (62) have investigated the effect of selectively boosting tumor regions above the base dose received by the entire tumor. They found that calculated values of TCP increased rapidly with both boost dose ratio and with proportion of volume boosted. The increase in TCP plateaued after boost dose ratios of 1.2-1.3 except where very large proportions of tumor volume exceeding 90% were boosted. Furthermore, quite large increases of TCP, to about 75%, could be achieved if the γ_{50} slope was steep, and especially in small tumors (having fewer cells). They concluded that there were few situations where a boost dose ratio exceeding 1.3 appeared to be worthwhile or necessary and that significant increase of TCP, up from 50% to 75%, might, therefore, be achieved for a small increase in risk of necrosis, where a substantial proportion of tumor volume (60-80%) could be boosted.

The discussion above assumes that the entire tumor is irradiated to some minimal base dose. In order to study and quantify the effect of a small volume of cold dose on TCP and effective uniform dose (EUD), Tomé and Fowler (63) constructed a four-bin DVH model in which the lowest dose bin, which has a fractional volume of 1%, is allowed to vary from 10% to 45% below prescription dose. As the dose deficit in the 1% subvolume bin increases further, it drives TCP and EUD rapidly down and can lead to a serious loss in TCP and EUD. Based on their study, a dose deficit to a 1% volume of the target that is larger than 20% of the prescription dose may lead to serious loss of TCP, even if a large volume of the target is boosted above the prescription dose, and hence, particular attention has to be paid to small-volume "cold" regions in the target. Furthermore, we conclude that the effect of cold regions on TCP can be minimized if the EUD associated with the target DVH is constrained to be equal to or larger than that of the intended prescription dose. Preliminary investigation suggests that helical tomotherapy appears to achieve better homogeneity for complex tumor volumes than linac-based IMRT or 3D conformal radiation therapy planning. (64) The avoidance of the potential consequences of "hot" and "cold" spots is being further explored specifically aiming to exploit the inherent advantages of helical tomotherapy.

Conclusions

Clinical implementation of IMRT, especially image-guided IMRT is in a state of rapid evolution. Helical tomotherapy, one the latest steps in this evolution, is an IMRT system whose design incorporates aspects such as infinite beam angle optimization and MVCT-based delivery verification. These features have the potential to permit the full clinical development of adaptive radiotherapy and conformal avoidance. To realize the ultimate goal of improving clinical outcomes for our patients, appropriate patient immobilization, optimized target localization, conformal avoidance of sensitive normal structures, and radiobiologically-guided dose escalation is required. The clinical implementation of helical tomotherapy, and the consequent issues raised (such as radiation dose-rates and dose homogeneity) present questions and opportunities that may change the current paradigm in radiation oncology.

Acknowledgements

This work was supported by NIH CA48902, NIH P01 CA088960.

References

- Mackie, T. R., Kapatoes, J., Ruchala, K., et al. Image-guidance for Precise Conformal Radiotherapy. *Int. J. Rad. Oncol. Biol. Phys.* 56, 89-105 (2003).
- Welsh, J. S., Patel, R. R., Ritter, M. A., Harari, P., Mackie, T. R., Mehta, M. P. Helical Tomotherapy: An Innovative Technology and Approach to Radiation Therapy. *Technol. Canc. Res. Treat.* 1, 55-63 (2002).
- Mackie, T. R., Balog, J., Ruchala, K. et al. Tomotherapy. *Sem. Radiat. Onc.* 9, 108-117 (1999).
- Welsh, J. S., Howard, S. P., Fowler, J. P. Dose-rate in External Beam Radiotherapy for Prostate Cancer – An Overlooked Confounding Variable? *Urology*. 62, 204-206 (2003).
- Fowler, J. F., Welsh, J. S., Howard, S. P. Loss of Biological Effect in Prolonged Fraction Delivery. *Int. J. Radiat. Oncol. Biol. Phys.* 59, 242-249 (2004).
- Low, D. A., Mutic, S., Dempsey, J. F. et al. Abutment Region Dosimetry for Serial Tomotherapy. *Int. J. Radiat. Oncol. Biol. Phys.* 45, 193-203 (1999).
- Carol, M., Bleier, A. R., et al. The Field-matching Problem as It Applies to the Peacock Three-dimensional Conformal System for Intensity Modulation. *Int. J. Radiat. Oncol. Biol. Phys.* 34, 183-187 (1996).
- Yan, D., Lockman, D., Brabbins, D., Tyburski, L., Martinez, A. An Off-line Strategy for Constructing a Patient-specific Planning Target Volume in Adaptive Treatment Process for Prostate Cancer. *Int. J. Radiat. Oncol. Biol. Phys.* 48, 289-302 (2000).
- Olivera, G. H., Fitchard, R. R., Reckwerdt, P. J., et al. Delivery Modification as an Alternative to Patient Repositioning in Tomotherapy. *Proc. 13th Int Conf on the Use of Computers in Radiation Therapy*, pp. 297-299. Eds., W. Schlegel and T. Borfeld. Heidelberg (2000).
- Welsh, J. S., Bradley, K., Manon, R., Lock, M., Patel, R., Ruchala, K., Mackie, T. R., Mehta, M. Megavoltage CT Imaging for Adaptive Helical Tomotherapy of Lung Cancer. *Clinical Lung Cancer* 5, 303-306 (2004).
- Ruchala, K., Olivera, G., Forrest, L., et al. Megavoltage CT for Image-guided Radiotherapy. *Radiotherapy and Oncology* 64 (Suppl.1), S12 (2002).
- Kapatoes, J. M., Olivera, G. H., Reckwerdt, P. J., et al. Delivery Verification in Sequential and Helical Tomotherapy. *Phys. Med. Biol.* 44, 1815-1841 (1999).
- Kapatoes, J. M., Olivera, G. H., Balog, J. P., et al. On the Accuracy and Effectiveness of Dose Reconstruction for Tomotherapy. *Phys. Med. Biol.* 46, 943-966 (2001).
- Van Dyke, J., Barnett, R. B., Cygler, J., et al. Commissioning and Quality Assurance of Treatment Planning Computers. *Int. J. Radiat. Oncol. Biol. Phys.* 26, 261-273 (1993).
- Low, D. A., Harms, W. B., Mutic, S., et al. A Technique for the Quantitative Evaluation of Dose Distributions. *Med. Phys.* 25, 656-661 (1998).
- Huguenin, P. U., Taussky, D., Moe, K., et al. Quality of Life in Patients Cured from a Carcinoma of the Head and Neck by Radiotherapy: The Importance of the Target Volume. *Int. J. Radiat. Oncol. Biol. Phys.* 45, 47-52 (1999).
- Chao, K. S. Protection of Salivary Function by Intensity-modulated Radiation Therapy in Patients with Head and Neck Cancer. *Sem. Radiat. Oncol.* 12 (S1), 20-25 (2002).
- Warde, P., O'Sullivan, B., Aslanidis, J., et al. A Phase III Placebo-controlled Trial of Oral Pilocarpine in Patients Undergoing Radiotherapy for Head-and-Neck Cancer. *Int. J. Radiat. Oncol. Biol. Phys.* 54, 9-13 (2002).
- Guchelaar, H. J., Vermes, A., Meerwaldt, J. H. Radiation-induced Xerostomia: Pathophysiology, Clinical Course and Supportive Treatment. *Supportive Care in Cancer* 5, 281-288 (1997).
- Brizel, D. M., Wasserman, T. H., Henke, M., et al. Phase III Randomized Trial of Amifostine as a Radioprotector in Head and Neck Cancer. *J. Clin. Oncol.* 18, 3339-3345 (2000).
- Kaneko, M., Shirato, H., Nishioka, T., et al. Scintigraphic Evaluation of Long-term Salivary Gland Function after Bilateral Whole Parotid Gland Irradiation in Radiotherapy for Head and Neck Tumour. *Oral Oncol.* 34, 140-146 (1998).
- Eisbruch, A., Kim, H. M., Terrell, J. E. et al. Xerostomia and its Predictors Following Parotid-sparing Irradiation of Head-and-Neck Cancer. *Int. J. Radiat. Oncol. Biol. Phys.* 50, 695-704 (2001).

23. Butler, E. B., The, B. S., Grant, W. H., et al. SMART (Simultaneous Modulated Accelerated Radiation Therapy) Boost: A New Accelerated Fractionation Schedule for the Treatment of Head and Neck Cancer with Intensity Modulated Radiotherapy. *Int. J. Radiat. Oncol. Biol. Phys.* 45, 21-32 (1999).
24. Nowak, P. J., Wijers, O. B., Lagerwaard, F. J., et al. A Three-dimensional CT-based Target Definition for Elective Irradiation of the Neck. *Int. J. Rad. Oncol. Biol. Phys.* 45, 33-39 (1999).
25. Wijers, O. B., Levendag, P. C., Tan, T., et al. A Simplified CT-based Definition of the Lymph Node Levels in the Node-negative Neck. *Radiother. Oncol.* 52, 35-42 (1999).
26. Ang, K. K., Thames, H. D. What Can be Expected from Elective Regional Radiotherapy? *Can. J. Sci. Am.* 5, 75-76 (1999).
27. Aldridge, J. S., Mackie, T. R. Conformal Avoidance Radiation Therapy. *Radiother. Oncol.* 48, S76 (1998).
28. Adams, W. M., Miller, P. E., Vail, D. M., et al. An Accelerated Technique for Irradiation of Malignant Canine Nasal and Paranasal Sinus Tumors. *Vet. Radiol. Ultrasound* 39, 475-481 (1998).
29. Welsh, J. S., Turek, M., Mackie, T. R., et al. Conformal Avoidance Helical Tomotherapy for Dogs with Nasopharyngeal Tumors. *Proc. 12th Int. Congr. Rad. Res.* 146 (abstr PP14/0447) (2003).
30. Booth, J. T., Zavgorodni, S. F. Set-up Error & Organ Motion Uncertainty: A Review. *Australasian Physical Eng. Sci. Med.* 22, 29-47 (1999).
31. Martel, M. K., Ten Haken, R. K., Hazuka, M. B., et al. Estimation of Tumor Control Probability Model Parameters From 3-D Dose Distributions of Non-Small Cell Lung Cancer Patients. *Lung Ca.* 24, 31-37 (1999).
32. Jones, L., Metcalfe, P., Hoban, P. Accounting for Treatment Delays When Treating Highly Proliferative Tumors. *Phys. Med. Biol.* 44, 223-234 (1999).
33. Horwitz, E. M., Hanlon, A. L., Pinover, W. H., et al. The Cost-effectiveness of 3D Conformal Radiation Therapy Compared with Conventional Techniques for Patients with Clinically Localized Prostate Cancer. *Int. J. Radiat. Oncol. Biol. Phys.* 45, 1219-1226 (1999).
34. Legorreta, A. P., Brooks, R. H., Leibowitz, A. N., et al. Cost of Breast Cancer Treatment. A 4-year Longitudinal Study. *Archives of Int. Med.* 156, 2197-2201 (1996).
35. Fowler, J. F., Chappell, R. Non-small Cell Lung Tumors Repopulate Rapidly During Radiation Therapy. *Int. J. Radiat. Oncol. Biol. Phys.* 46, 516-517 (2000).
36. Cox, J. D., Pajak, T. F., Asbell, S., et al. Interruptions of High-dose Radiation Therapy Decrease Long-term Survival of Favorable Patients with Unresectable Non-small Cell Carcinoma of the Lung: Analysis of 1244 Cases from 3 Radiation Therapy Oncology Group (RTOG) Trials. *Int. J. Radiat. Oncol. Biol. Phys.* 27, 493-498 (1993).
37. Kwa, S. L., Lebesque, J. V., Theuws, J. C., et al. Radiation Pneumonitis as a Function of Mean Lung Dose: An Analysis of Pooled Data of 540 Patients. *Int. J. Radiat. Oncol. Biol. Phys.* 42, 1-9 (1998).
38. Mehta, M., Scrimger, R., Mackie, T. R., Paliwal, B., Chappell, R., Fowler, J. A New Approach to Dose Escalation in Non-small Cell Lung Cancer. *Int. J. Radiat. Oncol. Biol. Phys.* 49, 23-33 (2001).
39. Withers, H. R., Taylor, J. M. G., Maciejewski, B. The Hazard of Accelerated Tumor Clonogen Repopulation During Radiotherapy. *Acta. Oncol.* 27, 131-146 (1988).
40. Roberts, S. A., Hendry, J. H. The Delay Before Onset of Accelerated Tumor Cell Repopulation During Radiotherapy: A Direct-maximum Likelihood Analysis of a Collection of Worldwide Tumor-control Data. *Radiother. Oncol.* 29, 69-74 (1993).
41. Brenner, D. J.. Accelerated Repopulation During Radiotherapy: Quantitative Evidence for Delayed Onset. *Radiat. Oncol. Invest.* 1, 167-172 (1993).
42. Scrimger, R. A., Tome, W. A., Olivera, G. H., Reckwerdt, P. J., Mehta, M. P., Fowler, J. F. Reduction in Radiation Doses to Lung and Other Normal Tissues Using Helical Tomotherapy to Treat Lung Cancer, in Comparison to Conventional Field Arrangements. *Am. J. Clin. Oncol.* 26, 70-78 (2003).
43. Hanks, G. E., Martz, K. L., Diamond, J. J. The Effect of Dose on Local Control of Prostate Cancer. *Int. J. Radiat. Oncol. Biol. Phys.* 15, 1299-1305 (1988).
44. Perez, C. A., Walz, B. J., Zivnuska, F. R., et al. Irradiation of Carcinoma of the Prostate Localized to the Pelvis: Analysis of Tumor Response and Prognosis. *Int. J. Radiat. Oncol. Biol. Phys.* 6, 555-563 (1980).
45. Pollack, A., Zagars, G. K., Smith, I. G., et al. Preliminary Results of a Randomized Dose-escalation Study Comparing 70 Gy to 78 Gy for the Treatment of Prostate Cancer. *Int. J. Radiat. Oncol. Biol. Phys.* 45, 146-147 (1999).
46. Hanks, G. E. Optimizing the Radiation Treatment and Outcome of Prostate Cancer. *Int. J. Radiat. Oncol. Biol. Phys.* 11, 1235-1245 (1985).
47. Michalski, J. M., Roach, M., Vijayakumar, S., et al. Preliminary Report of Toxicity Following 3D Radiation Therapy for Prostate Cancer on 3DOG/RTOG 9406. *Int. J. Radiat. Oncol. Biol. Phys.* 46, 391-402 (2000).
48. Zelefsky, M. J., Fuks, Z., Hunt, M., et al. High-dose Intensity Modulated Radiation Therapy for Prostate Cancer: Early Toxicity and Biochemical Outcome in 772 Patients. *Urol. Oncol.* 21, 306-307 (2003).
49. Haustermans, K. M. H., Hofland, I., van Poppel, H., et al. Cell Kinetic Measurements in Prostate Cancer. *J. Radiat. Oncol. Biol. Phys.* 197, 1067-1070.
50. Brenner, D. J., Hall, E. J. Fractionation and Protraction for Radiotherapy of Prostate Carcinoma. *Int. J. Radiat. Oncol. Biol. Phys.* 43, 1095-1101 (1999).
51. Fowler, J. J., Chappell, R., Ritter, M. *Int. J. Radiat. Oncol. Biol. Phys.* 50, 1021-1031 (2001).
52. Brenner, D. J., Martinez, A. A., Edmundson, G. K., et al. *Int J Radiat Oncol Biol Phys* 52, 6-13 (2002).
53. Duschesne, G. M., Peters, L. J. What is the Alpha/Beta Ratio for Prostate Cancer? Rationale for Hypofractionated High-Dose-Rate Brachytherapy. *J. Radiat. Oncol. Biol. Phys.* 44, 747-748 (1999).
54. Patel, R. R., Orton, N., Tome, W. A., et al. Rectal Dose Sparing with a Balloon Catheter and Ultrasound Localization in Conformal Radiation Therapy for Prostate Cancer. *Radiother. Oncol.* 67, 285-294 (2003).
55. Menke, M., Hirschfeld, F., Mack, T., et al. Photogrammetric Accuracy Measurements of Head Holder Systems used for Fractionated Radiotherapy. *Int. J. Radiat. Oncol. Biol. Phys.* 24, 781-787 (1992).
56. Delannes, M., Daly, N. J., Bonnet, J., et al. Fractionated Radiotherapy of Small Inoperable Lesions of the Brain Using a Noninvasive Stereotactic Frame. *Int. J. Radiat. Oncol. Biol. Phys.* 21, 749-755 (1991).
57. Laing, R. W., Thompson, V., Warrington, A. P., et al. Feasibility of Patient Immobilization for Conventional Cranial Irradiation with Relocatable Stereotactic Frame. *Br. J. Radiol.* 66, 1020-1024 (1993).
58. Tomé, W. A., Meeks, S. L., McNutt, T. R., et al. Optically Guided Intensity Modulated Radiotherapy. *Radiother. Oncol.* 61, 33-44 (2001).
59. Tomé, W. A., Meeks, S. L., Buatti, J. M., et al. A High-precision System for Conformal Intracranial Radiotherapy. *Int. J. Radiat. Oncol. Biol. Phys.* 47, 1137-1143 (2000).
60. Bouchet, L. G., Meeks, S. L., Goodchild, G. Calibration of Three-dimensional Ultrasound Images for Image-guided Radiation Therapy. *Phys. Med. Biol.* 46, 559-577 (2001).
61. Ford, E. C., Magera, G. S., Yorke, E., et al. Evaluation of Respiratory Movement During Gated Radiotherapy Using Film and Electronic Portal Imaging. *Int. J. Radiat. Oncol. Biol. Phys.* 52, 522-531 (2002).
62. Tomé, W. A., Fowler, J. F. Selective Boosting of Tumor Subvolumes. *Int. J. Radiat. Oncol. Biol. Phys.* 48, 593-599 (2000).
63. Tomé, W. A., Fowler, J. F. On Cold Spots in Tumor Subvolumes. *Med. Phys.* 29, 1590-1598 (2002).
64. Welsh, J., Olivera, G., Hui, S., et al. Helical Tomotherapy with Conformal Avoidance Appears Superior to 3-D CRT and IMRT for

- Treatment of Complex Tumor Volumes. *Radiother. Oncol.* 64 (suppl 1) S124 (2002).
65. Pouliot, J., Bani-Hashemi, A., Chen, J., Svatos, M., et al. Low-dose Megavoltage Cone-beam CT for Radiation Therapy. *Int. J. Radiat. Oncol. Biol. Phys.* 61, 552-560 (2005).
 66. Orton, N., Jaradat, H., Welsh, J. S., Tome, W. Whole Scalp Irradiation using Helical Tomotherapy. *Medical Dosimetry*. 30, 162-168 (2005).
 67. Khuntia, D., Jaradat, H., Orton, N., Mehta, M. P., Tome, W., Welsh, J. S. Helical Tomotherapy as a Means of Administering Total or Partial Scalp Irradiation. *Int. J. Radiat. Oncol. Biol. Phys.* 64, 1288-1289 (2006).
 68. Hui, S. K., Kapatoes, J., Fowler, J., Henderson, D., Olivera, G., Manon, R. R., Gerbi, B., Mackie, T. R., Welsh, J. S. Feasibility Study of Helical Tomotherapy for Total Body or Total Marrow Irradiation. *Med. Phys.* 32, 3214 (2005).
 69. Welsh, J. S., Peterson, C., Kahl, B., Olivera, G. Radiotherapy for Hodgkin's Disease and Non-Hodgkin's Lymphoma Using Intensity Modulated Radiation Therapy Via Helical Tomotherapy: A New Mantle. In *Intensity Modulated Radiation Therapy: A Clinical Perspective*. Eds., Mundt, A. J. and Roeske, J. C. BC Decker Inc Publishers (2005).
 70. Vineberg, K. A., Eisbruch, A., Coselmon, M. M., et al. Is Uniform Target Dose Possible in IMRT Plans in the Head and Neck? *Int. J. Radiat. Oncol. Biol. Phys.* 52, 1159-1172 (2002).

Received: June 26, 2006; Revised: August 24, 2006;

Accepted: September 2, 2006

